Wave-Packet Surface Propagation for Light-Induced Molecular Dynamics

Shengzhe Pan,[1] Zhaohan Zhang,[2] Chenxi Hu,[2] Peifen Lu,[1] Xiaochun Gong,[1,5] Ruolin Gong,[1] Wenbin Zhang,[1] Lianrong Zhou,[1] Chenxu Lu,[1] Menghang Shi,[1] Zhejun Jiang,[1] Hongcheng Ni,[1,5] Feng He,[2,3] and Jian Wu[1,3,4,5,*]

[1]*State Key Laboratory of Precision Spectroscopy, East China Normal University, Shanghai 200241, China*

[2]*Key Laboratory for Laser Plasmas (Ministry of Education) and School of Physics and Astronomy, Collaborative Innovation Center of IFSA (CICIFSA), Shanghai Jiao Tong University, Shanghai 200240, China*

[3]*CAS Center for Excellence in Ultra-intense Laser Science, Shanghai 201800, China*

[4]*Chongqing Key Laboratory of Precision Optics, Chongqing Institute of East China Normal University, Chongqing 401121, China*

[5]*Collaborative Innovation Center of Extreme Optics, Shanxi University, Taiyuan, Shanxi 030006, China*

(Received 7 May 2023; revised 5 October 2023; accepted 22 December 2023; published 17 January 2024)

Recent advances in laser technology have enabled tremendous progress in light-induced molecular reactions, at the heart of which the breaking and formation of chemical bonds are located. Such progress has been greatly facilitated by the development of an accurate quantum-mechanical simulation method, which, however, does not necessarily accompany clear dynamical scenarios and is rather computationally heavy. Here, we develop a wave-packet surface propagation (WASP) approach to describe the molecular bond-breaking dynamics from a hybrid quantum-classical perspective. Via the introduction of quantum elements including state transitions and phase accumulations to the Newtonian propagation of the nuclear wave packet, the WASP approach naturally comes with intuitive physical scenarios and accuracies. It is carefully benchmarked with the H_2^+ molecule and is shown to be capable of precisely reproducing experimental observations. The WASP method is promising for the intuitive visualization of light-induced molecular dynamics and is straightforward extensible towards complex molecules.

DOI: 10.1103/PhysRevLett.132.033201

Coherent control of molecular bond breakup and formation has been a heated topic of discussion lately thanks to recent advances in laser technology that make tailored intense laser pulses routinely available [1–5]. The ingeniously sculptured laser fields carry specific frequencies tailored to populate certain states and initiate controlled or steered chemical reactions [6–15], which have attracted much attention not only in physics and chemistry laboratories but also in interstellar space, e.g., the formation of trihydrogen cation as the initiator for most chemical reactions in interstellar clouds [16–19]. The molecular dynamics during chemical reactions can be, in principle, well described by quantum mechanics via the solution of the time-dependent Schrödinger equation (TDSE). However, even for the simplest neutral molecule of H_2, an *ab initio* numerical simulation is still challenging due to the large number of degrees of freedom involved in a molecular reaction. Furthermore, an intuitive physical picture remains evanescent even if an agreement with experimental results can be reached. Therefore, a general approach with low computational cost and a clear physical picture is highly desirable for describing molecular dynamical reactions under intense laser fields.

In this Letter, we develop an intuitive wave-packet surface propagation (WASP) approach to describe the light-induced dissociation dynamics of molecules. It is realized via the introduction of quantum elements including state transitions and phase accumulations into the classical propagation of nuclear wave packets (NWPs) on the potential energy surfaces of a stretching molecule. Using a classical description of the nuclear dynamics substantially alleviates the computational overhead, while keeping quantum elements during transitions preserves the essential physics crucial to light-induced chemical reactions. The WASP approach is carefully benchmarked against the H_2^+ molecule and is shown to be capable of precisely simulating experimental observations. In particular, the WASP model reproduces the feature-rich two-dimensional (2D) momentum distributions and the laser-phase-dependent directional ejection of the protons in the dissociative ionization of H_2 driven by an orthogonal two-color (OTC) laser pulse. The present WASP approach provides a hybrid quantum-classical perspective to precisely simulate the light-induced molecular dissociation, which is both highly efficient and physically transparent in comparison to *ab initio* quantum simulation methods.

The essence of the WASP model is the construction of the dissociating NWP via including the state transitions and phase accumulations to its classical propagation along various pathways as the molecule stretches, as

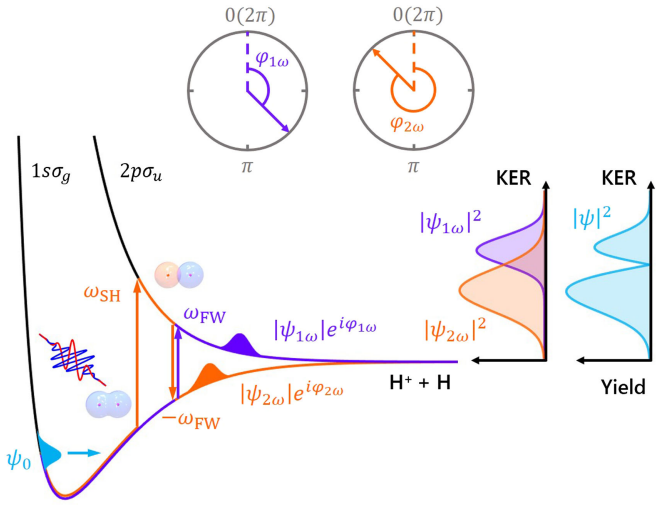

FIG. 1. Schematic illustration of light-induced dissociation dynamics of H_2^+ driven by an OTC laser field. Two black curves denote the potential energy curves of the electronic ground ($1s\sigma_g$) and excited ($2p\sigma_u$) states, respectively. The NWP on the ground state is launched by releasing one electron at the equilibrium internuclear distance of H_2, illustrated by the blue wave packet. The created NWP subsequently propagates on these two potential curves, and here two pathways, for example, are shown with different colors ($1\omega_{\mathrm{SH}} - 1\omega_{\mathrm{FW}}$ pathway in orange and $1\omega_{\mathrm{FW}}$ pathway in violet). Two dials with different colors denote the accumulated phases of the two pathways. The two panels on the right denote the KER spectra from the incoherent and coherent superposition of the two pathways, respectively.

schematically illustrated in Fig. 1 (taking the simplest molecule of H_2^+ as an example). The rotation of the molecular axis occurs on a timescale much longer than that of dissociation and thus is not considered here. The constructed 2D NWP superimposed from various dissociation pathways, as a function of the kinetic energy release (KER) E_n, molecular orientations θ_p, and laser phase ϕ_L, can be written as

$$\psi(E_n,\theta_p,\phi_L) = \sum_j \psi_J(E_n,\theta_p,\phi_L) = \sum_j [G_J(E_n) A_J(\theta_p,\phi_L) e^{-i\varphi_J}], \quad (1)$$

where ψ_J is the NWP for pathway J. Here the kinetic energy distribution G_J of a dissociating NWP upon absorption and emission of photons is mainly introduced by considering the spectrum width of the ultrashort laser pulse. Thus the width of the kinetic energy distribution becomes shorter when a longer laser pulse (with a narrower spectrum) is implemented. Meanwhile, if the NWP absorbs or emits more photons during the dissociation, it will end with a narrower kinetic energy distribution taking high-order nonlinear processes into account. The initial NWP is launched at the equilibrium internuclear distance R_0 of the neutral target molecule upon electron removal at the peak of the laser pulse. The subsequent propagation of the NWP on the potential energy curves of the cation is described as the Newtonian motion of a classical particle by the force $F = -\mathrm{d}V(R)/\mathrm{d}R$ [20]. The initial kinetic energy of the NWP is set to match the resonant dissociation condition, i.e., the NWP has enough kinetic energy to approach the internuclear distance of the resonant transition.

The dissociating NWPs of different pathways with the same KER would interfere with each other, carrying individual phases φ_J accumulated along the respective dissociation pathways, which leads to the rich structure of the observed KER spectrum on the detector, as illustrated in the right panel of Fig. 1. The accumulated phase of a specific dissociation pathway is described as follows [21]:

$$\varphi_J = -\sum_{k=1}^{n} E_k \Delta t_k + \sum_{k=1}^{n-1} (-1)^k \omega_k t_k + \sum_{k=1}^{n-1} (-1)^{k-1} \pi + \int_{R_0}^{R_\infty} p_J(R)\mathrm{d}R, \quad (2)$$

where the first term originates from the phase evolution of the NWP with the system energy E_k and corresponding propagation time Δt_k on the eigenstate, the second term originates from the phase evolution of the laser pulse with the absorption or emission of the photons ω_k, the third term denotes the phase associated with the symmetry change of the electronic wave function upon quantum-state transitions, and the last term denotes the phase accumulated from the classical motion of the NWP on the potential energy curves with its classical momentum p_J, integrated from the initial internuclear distance R_0 to an infinite internuclear distance R_∞. With the classical propagation dynamics and phase accumulations at hand, the core of the WASP model is to construct the overall transition amplitude A_J, including all involved transitions in a specific dissociation pathway, which ranges from one-photon to multiphoton process driven by strong laser fields. Hence, we derive the amplitude of nonlinear multiphoton transitions from a unified model of Rabi oscillations beyond the perturbation theory [22–25] (see Appendix and Supplemental Material [26] for derivation details).

To evaluate the accuracy of a numerical method, we compare the simulation results with the experimental observations. Experimentally, a cold-target recoil ion momentum spectroscopy reaction microscope [51,52] is employed to measure the momenta of the proton from the dissociation of H_2^+ driven by an OTC femtosecond laser pulse (see Supplemental Material [26] for experimental details). Figure 2(a) shows the measured 2D momentum distribution of the ejected protons with the OTC polarization shown in the inset. Here the peak intensity of the y-polarized second harmonic (SH) pulse is $I_{\mathrm{SH}} = 4 \times 10^{13}$ W/cm^2 and the peak intensity of the z-polarized fundamental wave (FW)

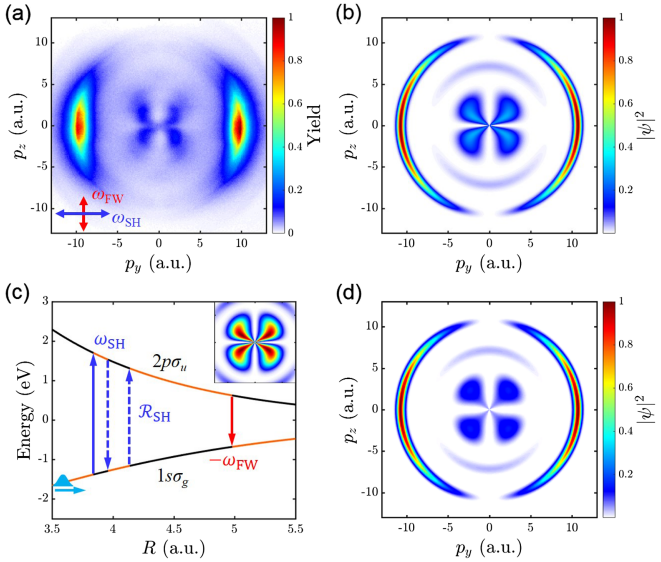

FIG. 2. (a) Measured momentum distribution of ejected protons driven by the OTC pulse. The SH and FW pulses are polarized along the y axis and z axis, respectively. (b) Simulated momentum distribution of ejected protons driven by the OTC pulse. (c) Schematic illustration of the $1\omega_{SH} + 1\mathcal{R}_{SH} - 1\omega_{FW}$ pathway contributing to the production of the very low-energy protons of the butterfly structure shown as the inset. Here blue and solid red arrows denote the $1\omega_{SH}$ absorption and $1\omega_{FW}$ emission, respectively. Two blue dashed arrows denote the dynamical Rabi coupling driven by the SH field, termed as $\mathcal{R}_{SH}$, where the bound electron jumps between the two electronic states. (d) Simulated momentum distribution of protons driven by the OTC pulse without the dynamical Rabi coupling. The maxima of all the momentum distributions are normalized to one for the convenience of comparison.

pulse is $I_{FW} = 1 \times 10^{12}$ W/cm^2. The numerical result is obtained by the present WASP model with the same OTC pulse, as shown in Fig. 2(b), which agrees very well with experimental observations. In the simulation, the 2D momentum distribution is averaged over the carrier-envelope phase of the FW pulse ϕ_{CEP} and the two-color relative phase ϕ_{TCP} to reach a consensus with the experimental measurement without the carrier-envelope phase locking. We have also confirmed that the focal-volume averaging effect hardly influences the 2D momentum distribution except for a slight relative yield difference of various channels. With the intuitive physical picture offered by the present WASP approach, we can infer relevant dissociation pathways involved in the molecular dissociation process. The high-energy protons with a momentum of 10.7 a.u. (KER $\sim$ 1.7 eV) ejecting along the y axis (0°) in Figs. 2(a) and 2(b) are mainly produced from the dissociation of the $1\omega_{SH}$ pathway (the NWP moving outwards on the $1s\sigma_g$ curve, followed by absorbing one photon of ω_{SH} and dissociating along the $2p\sigma_u$ curve). The low-energy protons with a momentum of 7.3 a.u. (KER $\sim$ 0.8 eV) ejecting along the z axis (90°) in Fig. 2(b) are attributed to the $1\omega_{FW}$ pathway (the NWP moving outwards on the $1s\sigma_g$ curve, followed by absorbing one photon of ω_{FW} and dissociating along the $2p\sigma_u$ curve).

The most prominent feature of the proton momentum distribution in Fig. 2(a) is the butterfly structure at very low energy (KER < 0.4 eV with momenta less than 5.2 a.u.) originating from the conjunct driving of the orthogonally polarized FW and SH fields, which is verified by individually switching off the FW or SH pulse in the WASP simulation (see Supplemental Material [26] for details). It is mainly produced via the $1\omega_{SH} - 1\omega_{FW}$ pathway, i.e., the NWP propagating outwards on the $1s\sigma_g$ curve first transits to and propagates along the $2p\sigma_u$ state by absorbing one photon of ω_{SH}, subsequently deexcites back to the $1s\sigma_g$ state by emitting one photon of ω_{FW} and eventually dissociate along the $1s\sigma_g$ curve. For the OTC laser field, the protons produced in the $1\omega_{SH} - 1\omega_{FW}$ dissociation pathway mainly eject along 45° due to the equal intensity dependence on the two orthogonal laser fields. However, as shown in the enlargement in Fig. 2(c), the butterfly structure is not strictly along 45° but slightly bends with a trend towards the y axis with decreasing momenta, which is attributed to stronger couplings with the y-polarized SH field (whose intensity is stronger than the z-polarized FW field, thus inducing more nonlinear couplings). This effect is modeled by the dynamical Rabi couplings in our WASP simulation. Figure 2(c) shows a schematic illustration of a typical two-color dissociation pathway with the dynamical Rabi coupling, named $1\omega_{SH} + 1\mathcal{R}_{SH} - 1\omega_{FW}$ pathway. After the NWP absorbs one photon of ω_{SH}, it may hop two times between two electronic states, resulting in one up-down cycle of dynamical Rabi couplings driven by the SH field, followed by the emission of one photon of ω_{FW} at a larger internuclear distance. An increase in the cycle number of dynamical Rabi couplings leads to a decrease in the KER of the dissociative fragments and an increased intensity dependence on the laser field [53]. By switching off the dynamical Rabi couplings in the WASP simulation, as shown in Fig. 2(d), the proton yield at very low kinetic energy dramatically decreases, and the above-observed butterfly structure becomes strictly along 45°. Thus, the protons in the near-zero KER region are produced by the strong dynamic Rabi couplings of the SH field, which drives the up-down hopping of the NWP many times between two electronic states. This physics, however, cannot be understood or reproduced in the well-known resonant transition scenario. Thanks to the unified model of strong-field-induced Rabi oscillations, we naturally consider the off-resonant transition amplitude with the detuning in molecular systems. The introduction of dynamical Rabi couplings reproduces the experimental observations and provides an intuitive physical picture. The 2D momentum distribution of the protons shown here is also benchmarked against the full-quantum simulation by numerically solving the TDSE (see Supplemental Material [26] for details).

Beyond the phase-averaged momentum distributions, directional breaking of the molecular bonds, strongly depending on the laser phase, is essential for the stereochemical reaction, providing a straightforward route to control the fate of molecules. To demonstrate the directional bond breaking, we slightly adjust the laser intensities to be $I_{\mathrm{SH}} = 6 \times 10^{12}$ and $I_{\mathrm{FW}} = 8 \times 10^{13}$ W/cm^2 so that more dissociation pathways with opposite parities participate with appropriate yields. The degree of the directional bond breaking is quantified by calculating the normalized differential yield of the protons emitting in one direction at a specific two-color phase of ϕ_{TCP}. The electron localized at the left or right nucleus (relative to a horizontally placed molecule) is determined by the coherent superposition of the NWPs on all gerade and ungerade states, i.e., $\psi_{\mathrm{left}} = \sum \psi_g + \sum \psi_u$ and $\psi_{\mathrm{right}} = \sum \psi_g - \sum \psi_u$. We can further obtain the probabilities by measuring the electron localized at the left or right nucleus via $P_{\mathrm{left}} = |\psi_{\mathrm{left}}|^2$ and $P_{\mathrm{right}} = |\psi_{\mathrm{right}}|^2$. Therefore, the two-dimensional asymmetry distribution of the ejected proton can be calculated as [6,8]

$$\mathcal{A}(E_k,\theta_p,\phi_{\mathrm{TCP}}) = \frac{P_{\mathrm{left}}(E_k,\theta_p,\phi_{\mathrm{TCP}}) - P_{\mathrm{right}}(E_k,\theta_p,\phi_{\mathrm{TCP}})}{P_{\mathrm{left}}(E_k,\theta_p,\phi_{\mathrm{TCP}}) + P_{\mathrm{right}}(E_k,\theta_p,\phi_{\mathrm{TCP}})}. \tag{3}$$

The measured and WASP simulated asymmetric distributions of the ejected protons as a function of the relative phase ϕ_{TCP} and the KER are shown in Figs. 3(a) and 3(b). Here, we select the molecular orientation of $30° < \theta_p < 60°$ to demonstrate the asymmetric distributions at different KER regions. Asymmetric structures are visible for the low-energy and high-energy regions as a function of the relative phase ϕ_{TCP}. The corresponding laser-phase-dependent asymmetries integrated over the regions of 0.4 eV < KER < 0.6 eV and 1.2 eV < KER < 1.4 eV are shown in the top panels. The phase shift of $\sim\pi/2$ is clearly observed from the two oscillatory curves. The main asymmetric distribution and the phase shift in simulated results are well in line with the experimental measurements. Furthermore, our WASP model can provide a physically transparent route to uncover quantum interferences in light-induced molecular dissociation via coherently or incoherently superimposing outgoing NWPs (see Supplemental Material [26] for details).

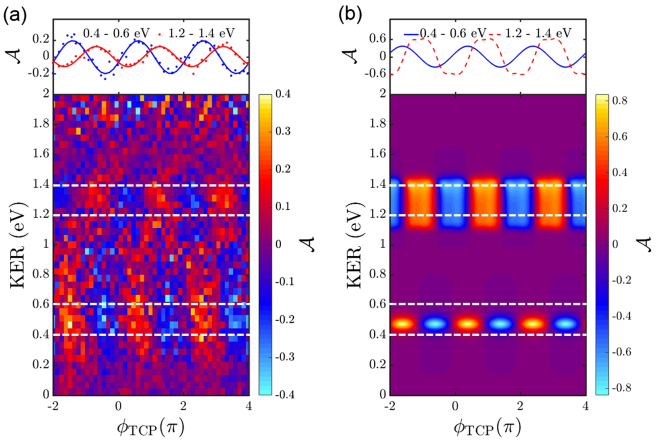

FIG. 3. (a) Measured two-dimensional maps of asymmetric distribution as a function of the two-color relative phase ϕ_{TCP} of the OTC pulse and KER of the ejected protons within the range of $30° < \theta_p < 60°$. (b) Simulated two-dimensional map of the asymmetric distribution as in (a). Two KER regions with clear asymmetries are indicated between the white dashed lines, the asymmetries of which are plotted in the top panels.

To demonstrate the general applicability of the WASP approach in modeling the light-induced dynamics of complex molecules, we provide two typical examples of a multielectron diatomic molecule of CO^+ and an organic molecule of $C_2H_2^{2+}$. In comparison to the simplest H_2^+ molecule, the potential energy curves of CO^+ may couple with each other due to the multielectron effect (see Supplemental Material [26] for calculation details), e.g., the avoided crossing between $D^2\Pi$ and $3^2\Pi$ states, as shown in Fig. 4(a). The experiments were performed on the CO molecule using an OTC laser field with the intensities $I_{\mathrm{SH}} = 4 \times 10^{13}$ and $I_{\mathrm{FW}} = 3 \times 10^{14}$ W/cm^2. The neutral CO molecule is singly ionized by the external laser field and the produced CO^+ subsequently dissociates into C^+ and O, where only the charged fragments C^+ can be measured in experiments, as shown in Fig. 4(b). The experimentally observed fine peaks are in accordance with the vibrational levels of the $A^2\Pi$ state. Thus, we perform the WASP simulation initialized from different vibrational states on the $A^2\Pi$ curve with corresponding Franck-Condon factors. These NWPs with different initial kinetic energies absorb photons from the OTC field, transit to the $D^2\Pi$, $3^2\Pi$, and $4^2\Pi$ states, and finally dissociate along two dissociation limits. The simulated 2D momentum distributions shown in Fig. 4(c) capture the essence of the experimental observations, where the central low-energy nuclear fragments are produced by the dynamical Rabi couplings between the diabatic $3^2\Pi$ potential energy curve and the $A^2\Pi$ curve, initialized at the low vibrational states of the $A^2\Pi$ curve.

Furthermore, the potential energy surfaces of the polyatomic molecule $C_2H_2^{2+}$ are complex due to the various motion modes of the four nuclei. Here we focus on the C—C bond stretching mode so that the dissociation can degenerate to the motion on a one-dimensional potential energy curve [54], as shown in Fig. 4(d) (see Supplemental Material [26] for calculation details). Analogously, we performed the experiments on the target of acetylene molecules using an OTC laser field with intensities $I = 5 \times 10^{13}$ and $I_{\mathrm{FW}} = 2 \times 10^{13}$ W/cm^2. The intense laser field may liberate two HOMO electrons of the neutral molecule and populate the NWPs on the $^3\Sigma_g^-$ state. There is

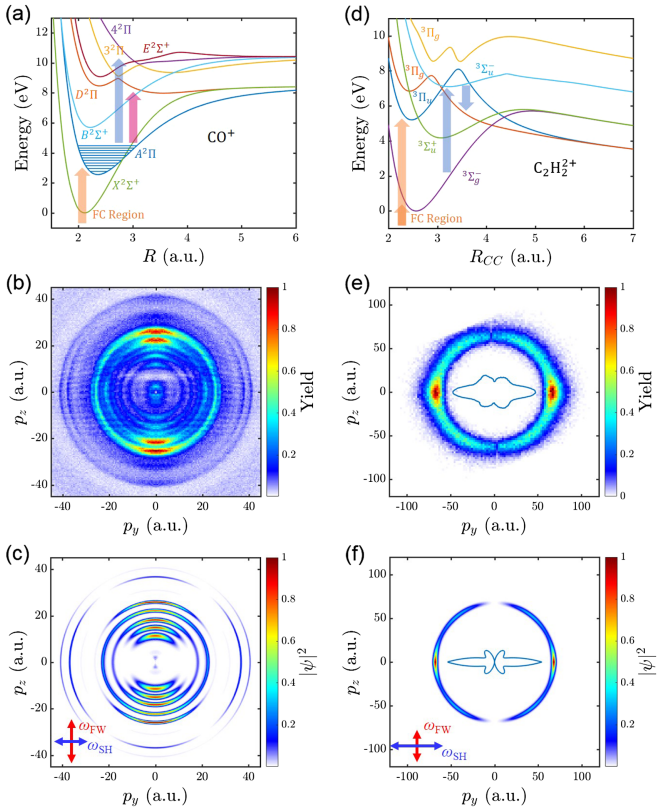

FIG. 4. (a) Relevant potential energy curves of CO^+. (b) Measured and (c) simulated momentum distributions of the ejected C^+ from the dissociation of CO^+: $CO^+ \rightarrow C^+ + O$ driven by an OTC laser pulse. (d) Relevant potential energy curves of $C_2H_2^{2+}$ with the C-C bond stretching. (e) Measured and (f) simulated momentum distributions of the ejected CH^+ from the dissociation of $C_2H_2^{2+}$: $C_2H_2^{2+} \rightarrow CH^+ + CH^+$ driven by an OTC laser pulse. The maxima of all the momentum distributions are normalized to one for the convenience of comparison.

also an appreciable probability that the laser field liberates one HOMO electron and one HOMO-1 (or HOMO-2) electron and populates the NWPs on the $^3\Pi_u$ or $^3\Pi_g$ states [55–57]. The produced $C_2H_2^{2+}$ subsequently dissociates into two CH^+, which can be detected in experiments and shown in Fig. 4(e). The four-leaf clover structure may be attributed to the convolution of parallel and perpendicular transitions. In addition, the strong parallel transition driven by the SH field is attributed to the strong coupling between the $^3\Pi_u$ and $^3\Pi_g$ states. We thus perform the WASP simulation considering the different ionization potentials of the populated states, from which the simulation results are shown in Fig. 4(f). We find that the NWP moving outwards on the $^3\Sigma_g^-$ curve absorbs photons to the $^3\Pi_u$ or $^3\Pi_u$ intermediate state and then emits one photon, ending with the dissociation along the $^3\Pi_g$ state. In each dissociation pathway, parallel and perpendicular transitions are involved, resulting in the four-leaf clover structure. Thus, a sharper horizontal structure is formed due to interference between the hybrid and strong parallel pathways.

In conclusion, we have developed a WASP approach to simulate molecular dynamics ranging from the weak-field one-photon process to strong-field multiphoton interactions. We utilize the basic concept of Rabi oscillations in quantum optics to naturally introduce the detunings of time-dependent energy levels and to construct nonlinear transition amplitudes beyond the perturbation theory [22–25]. By introducing these nonlinear transition amplitudes and phase accumulations to the classical propagation of the NWP on involved potential energy surfaces, the WASP approach combines the advantages of the clarity of a classical description and the precision of quantum evolution and thus can accurately predict the ionic momentum distributions of several typical molecules, verified by our experiments and full-quantum simulations. The transparent WASP model allows us to understand the physics of the experimentally observed butterfly structure in H_2^+ molecule and reveals many physical insights in complex molecules such as the universal dynamical Rabi couplings, the convolution of parallel and perpendicular transitions, and the multipathway quantum interference in an intuitive manner. The present WASP model features highly improved calculation efficiency with considerable accuracy, clear physical scenarios instead of black-box nature, and general applicability towards complex molecules, which is expected to become a standard simulation method focusing on light-molecule interactions.

This work was supported by the National Natural Science Foundation of China (Grants No. 12227807, No. 12241407, No. 11925405, No. 92150105, and No. 12304377); the Science and Technology Commission of Shanghai Municipality (Grants No. 23JC1402000, No. 21ZR1420100 and No. 23PJ1402600).

Appendix: Nonlinear multiphoton transitions.—For the one-photon process in molecular systems, the transition amplitude can be formulated as $A_{1\omega} = \Omega_{1\omega}\tau_{1\omega}$, where $\Omega_{1\omega} = D(R_{1\omega})\mathcal{E}(t)/2$ is defined as the one-photon laser-molecule coupling at the resonant distance $R_{1\omega}$ with the dipole D and the laser field strength $\mathcal{E}$, and $\tau_{1\omega}$ denotes the effective duration of the one-photon transition in a molecule. Analogously, the overall multiphoton transition amplitude, e.g., the transition amplitude of the net-two-photon dissociation pathway of H_2^+, can be deduced by combining the three-photon absorption at $R_{3\omega}$ and the one-photon emission at $R_{1\omega}$, resulting in $A_{2\omega} = (\Omega_{3\omega}/2\omega)(\Omega_{3\omega}/2\omega)\Omega_{3\omega}(\Omega_{1\omega}/\Delta V_{u(31)})\tau_{2\omega}$. Here $\Omega_{3\omega} = D(R_{3\omega})\mathcal{E}(t)/2$ denotes the dipole interaction at the three-photon resonant internuclear distance $R_{3\omega}$, $\tau_{2\omega}$ denotes the effective duration of the net-two-photon dissociation pathway, and the intermediate detuning of the subsequent one-photon emission is given by $\Delta V_{u(31)} = V_u(R_{3\omega}) - V_u(R_{1\omega})$ with V_u being the potential energy

curve of the $2p\sigma_u$ state. The nonlinear transition amplitude has been benchmarked and confirmed in experiments using a single near-infrared laser pulse (see Supplemental Material [26] for details), where the yield ratio of the net-two-photon pathway to the one-photon pathway has been utilized to calibrate the laser intensity of the interaction region [58]. For the dynamical Rabi coupling in molecular systems, the electron continuously hops between two electronic states governed by the area theorem driven by the laser pulse [53,59,60]. Consequently, the transition amplitude of the one-photon-one-Rabi-coupling pathway can be described as $A_{1\omega-1\mathcal{R}} = \Omega_{1\omega}(\Omega_{\mathcal{R}_1}/\Delta V_{g(11')})(\Omega_{\mathcal{R}_2}/\Delta V_{u(12')})\tau_{1\omega-1\mathcal{R}}$, where the intermediate detunings of the subsequent off-resonant transitions are defined as $\Delta V_{g(11')} = -V_g(R_{1\omega}) + V_g(R_{\mathcal{R}_1})$ and $\Delta V_{u(12')} = V_u(R_{1\omega}) - V_u(R_{\mathcal{R}_2})$.

*jwu@phy.ecnu.edu.cn

[1] B. Sheehy and L. F. DiMauro, Atomic and molecular dynamics in intense optical fields, Annu. Rev. Phys. Chem. **47**, 463 (1996).

[2] J. H. Posthumus, The dynamics of small molecules in intense laser fields, Rep. Prog. Phys. **67**, 623 (2004).

[3] M. F. Kling, P. von den Hoff, I. Znakovskaya, and R. de Vivie-Riedle, Sub-femtosecond control of molecular reactions via tailoring the electric field of light, Phys. Chem. Chem. Phys. **15**, 9448 (2013).

[4] A. S. Alnaser and I. V. Litvinyuk, Sub-femtosecond directional control of chemical processes in molecules, J. Phys. B **50**, 032002 (2017).

[5] H. Ibrahim, C. Lefebvre, A. D. Bandrauk, A. Staudte, and F. Légaré, H_2: The benchmark molecule for ultrafast science and technologies, J. Phys. B **51**, 042002 (2018).

[6] M. F. Kling, C. Siedschlag, A. J. Verhoef, J. I. Khan, M. Schultze, T. Uphues, Y. Ni, M. Uiberacker, M. Drescher, F. Krausz, and M. J. J. Vrakking, Control of electron localization in molecular dissociation, Science **312**, 246 (2006).

[7] M. Kremer, B. Fischer, B. Feuerstein, V. L. B. de Jesus, V. Sharma, C. Hofrichter, A. Rudenko, U. Thumm, C. D. Schröter, R. Moshammer, and J. Ullrich, Electron localization in molecular fragmentation of H_2 by carrier-envelope phase stabilized laser pulses, Phys. Rev. Lett. **103**, 213003 (2009).

[8] D. Ray, F. He, S. De, W. Cao, H. Mashiko, P. Ranitovic, K. P. Singh, I. Znakovskaya, U. Thumm, G. G. Paulus, M. F. Kling, I. V. Litvinyuk, and C. L. Cocke, Ion-energy dependence of asymmetric dissociation of D_2 by a two-color laser field, Phys. Rev. Lett. **103**, 223201 (2009).

[9] B. Fischer, M. Kremer, T. Pfeifer, B. Feuerstein, V. Sharma, U. Thumm, C. D. Schröter, R. Moshammer, and J. Ullrich, Steering the electron in H_2^+ by nuclear wave packet dynamics, Phys. Rev. Lett. **105**, 223001 (2010).

[10] I. Znakovskaya, P. von den Hoff, G. Marcus, S. Zherebtsov, B. Bergues, X. Gu, Y. Deng, M. J. J. Vrakking, R. Kienberger, F. Krausz, R. de Vivie-Riedle, and M. F. Kling, Subcycle controlled charge-directed reactivity with few-cycle midinfrared pulses, Phys. Rev. Lett. **108**, 063002 (2012).

[11] A. Fischer, A. Sperl, P. Cörlin, M. Schönwald, H. Rietz, A. Palacios, A. González-Castrillo, F. Martín, T. Pfeifer, J. Ullrich, A. Senftleben, and R. Moshammer, Electron localization involving doubly excited states in broadband extreme ultraviolet ionization of H_2, Phys. Rev. Lett. **110**, 213002 (2013).

[12] N. G. Kling, K. J. Betsch, M. Zohrabi, S. Zeng, F. Anis, U. Ablikim, B. Jochim, Z. Wang, M. Kübel, M. F. Kling, K. D. Carnes, B. D. Esry, and I. Ben-Itzhak, Carrier-envelope phase control over pathway interference in strong-field dissociation of H_2^+, Phys. Rev. Lett. **111**, 163004 (2013).

[13] X. Xie, T. Wang, S. G. Yu, X. Y. Lai, S. Roither, D. Kartashov, A. Baltuška, X. J. Liu, A. Staudte, and M. Kitzler, Disentangling intracycle interferences in photoelectron momentum distributions using orthogonal two-color laser fields, Phys. Rev. Lett. **119**, 243201 (2017).

[14] S. Kangaparambil, V. Hanus, M. Dorner-Kirchner, P. He, S. Larimian, G. Paulus, A. Baltuška, X. Xie, K. Yamanouchi, F. He, E. Lötstedt, and M. Kitzler-Zeiler, Generalized phase sensitivity of directional bond breaking in the laser-molecule interaction, Phys. Rev. Lett. **125**, 023202 (2020).

[15] H. Li, X. Gong, H. Ni, P. Lu, X. Luo, J. Wen, Y. Yang, X. Qian, Z. Sun, and J. Wu, Light-induced ultrafast molecular dynamics: From photochemistry to optochemistry, J. Phys. Chem. Lett. **13**, 5881 (2022).

[16] S. Miller, J. Tennyson, T. R. Geballe, and T. Stallard, Thirty years of H_3^+ astronomy, Rev. Mod. Phys. **92**, 035003 (2020).

[17] B. A. McGuire, O. Asvany, S. Brünken, and S. Schlemmer, Laboratory spectroscopy techniques to enable observations of interstellar ion chemistry, Nat. Rev. Phys. **2**, 402 (2020).

[18] Y. Mi, E. Wang, Z. Dube, T. Wang, A. Yu. Naumov, D. M. Villeneuve, P. B. Corkum, and A. Staudte, D_3^+ formation through photoionization of the molecular $D_2 - D_2$ dimer, Nat. Chem. **15**, 1224 (2023).

[19] L. Zhou, H. Ni, Z. Jiang, J. Qiang, W. Jiang, W. Zhang, P. Lu, J. Wen, K. Lin, M. Zhu, R. Dörner, and J. Wu, Ultrafast formation dynamics of D_3^+ from the light-driven bimolecular reaction of the $D_2 - D_2$ dimer, Nat. Chem. **15**, 1229 (2023).

[20] I. A. Bocharova, A. S. Alnaser, U. Thumm, T. Niederhausen, D. Ray, C. L. Cocke, and I. V. Litvinyuk, Time-resolved Coulomb-explosion imaging of nuclear wave-packet dynamics induced in diatomic molecules by intense few-cycle laser pulses, Phys. Rev. A **83**, 013417 (2011).

[21] J. Wu, M. Magrakvelidze, L. Ph. H. Schmidt, M. Kunitski, T. Pfeifer, M. Schöffler, M. Pitzer, M. Richter, S. Voss, H. Sann, H. Kim, J. Lower, T. Jahnke, A. Czasch, U. Thumm, and R. Dörner, Understanding the role of phase in chemical bond breaking with coincidence angular streaking, Nat. Commun. **4**, 2177 (2013).

[22] A. Giusti-Suzor, X. He, O. Atabek, and F. H. Mies, Above-threshold dissociation of H_2^+ in intense laser fields, Phys. Rev. Lett. **64**, 515 (1990).

[23] P. H. Bucksbaum, A. Zavriyev, H. G. Muller, and D. W. Schumacher, Softening of the H_2^+ molecular bond in intense laser fields, Phys. Rev. Lett. **64**, 1883 (1990).

[24] K. Sändig, H. Figger, and T. W. Hänsch, Dissociation dynamics of H_2^+ in intense laser fields: Investigation of photofragments from single vibrational levels, Phys. Rev. Lett. **85**, 4876 (2000).

[25] J. McKenna, A. M. Sayler, F. Anis, B. Gaire, Nora G. Johnson, E. Parke, J. J. Hua, H. Mashiko, C. M. Nakamura, E. Moon, Z. Chang, K. D. Carnes, B. D. Esry, and I. Ben-Itzhak, Enhancing high-order above-threshold dissociation of H_2^+ beams with few-cycle laser pulses, Phys. Rev. Lett. **100**, 133001 (2008).

[26] See Supplemental Material at http://link.aps.org/supplemental/10.1103/PhysRevLett.132.033201, which includes Refs. [27–50] for a detailed description of the WASP model, experiments, and TDSE simulations.

[27] I. I. Rabi, On the process of space quantization, Phys. Rev. **49**, 324 (1936).

[28] V. M. Akulin and N. V. Karlov, *Intense Resonant Interactions in Quantum Electronics* (Springer-Verlag, Berlin, 1992).

[29] H. Mashiko, S. Gilbertson, C. Li, S. D. Khan, M. M. Shakya, E. Moon, and Z. Chang, Double optical gating of high-order harmonic generation with carrier-envelope phase stabilized lasers, Phys. Rev. Lett. **100**, 103906 (2008).

[30] M. Chini, H. Mashiko, H. Wang, S. Chen, C. Yun, S. Scott, S. Gilbertson, and Z. Chang, Delay control in attosecond pump-probe experiments, Opt. Express **17**, 21459 (2009).

[31] X. Gong, P. He, Q. Song, Q. Ji, H. Pan, J. Ding, F. He, H. Zeng, and J. Wu, Two-dimensional directional proton emission in dissociative ionization of H_2, Phys. Rev. Lett. **113**, 203001 (2014).

[32] K. Lin, X. Gong, Q. Song, Q. Ji, W. Zhang, J. Ma, P. Lu, H. Pan, J. Ding, H. Zeng, and J. Wu, Directional bond breaking by polarization-gated two-color ultrashort laser pulses, J. Phys. B **49**, 025603 (2016).

[33] W. Zhang, H. Li, K. Lin, P. Lu, X. Gong, Q. Song, Q. Ji, J. Ma, H. Li, H. Zeng, F. He, and J. Wu, Photon-number-resolved asymmetric dissociative single ionization of H_2, Phys. Rev. A **96**, 033405 (2017).

[34] Z.-H. Zhang, Y. Li, Y.-J. Mao, and F. He, QPC-TDSE: A parallel TDSE solver for atoms and small molecules in strong lasers. Comput. Phys. Commun. **290**, 108787 (2023).

[35] D. Ursrey, F. Anis, and B. D. Esry, Multiphoton dissociation of HeH^+ below the $He^+(1\,s) + H(1\,s)$ threshold, Phys. Rev. A **85**, 023429 (2012).

[36] B. Fetić, W. Becker, and D. B. Milošević, Extracting photoelectron spectra from the time-dependent wave function: Comparison of the projection onto continuum states and window-operator methods, Phys. Rev. A **102**, 023101 (2020).

[37] K. P. Singh, F. He, P. Ranitovic, W. Cao, S. De, D. Ray, S. Chen, U. Thumm, A. Becker, M. M. Murnane, H. C. Kapteyn, I. V. Litvinyuk, and C. L. Cocke, Control of electron localization in deuterium molecular ions using an attosecond pulse train and a many-cycle infrared pulse, Phys. Rev. Lett. **104**, 023001 (2010).

[38] X. Urbain, B. Fabre, E. M. Staicu-Casagrande, N. de Ruette, V. M. Andrianarijaona, J. Jureta, J. H. Posthumus, A. Saenz, E. Baldit, and C. Cornaggia, Intense-laser-field ionization of molecular hydrogen in the tunneling regime and its effect on the vibrational excitation of H_2^+, Phys. Rev. Lett. **92**, 163004 (2004).

[39] A. Rudenko, Th. Ergler, B. Feuerstein, K. Zrost, C. D. Schröter, R. Moshammer, and J. Ullrich, Real-time observation of vibrational revival in the fastest molecular system, Chem. Phys. **329**, 193 (2006).

[40] F. He and U. Thumm, Dissociative ionization of H_2 in an attosecond pulse train and delayed laser pulse, Phys. Rev. A **81**, 053413 (2010).

[41] P. M. Abanador, T. Pauly, and U. Thumm, Molecular bond stabilization in the strong-field dissociation of O_2^+, Phys. Rev. A **101**, 043410 (2020).

[42] H.-J. Werner, P. J. Knowles *et al.*, MOLPRO, version 2012.1, 2012.

[43] H.-J. Werner and P. J. Knowles, An efficient internally contracted multiconfiguration-reference configuration interaction method, J. Chem. Phys. **89**, 5803 (1988).

[44] D. E. Woon and T. H. Dunning Jr., Gaussian basis sets for use in correlated molecular calculations. V. Core-valence basis sets for boron through neon, J. Chem. Phys. **103**, 4572 (1995).

[45] K. Okada and S. Iwata, Accurate potential energy and transition dipole moment curves for several electronic states of CO^+, J. Chem. Phys. **112**, 1804 (2000).

[46] S. L. Guberman, Potential curves for the dissociative recombination of CO^+, J. Phys. Chem. A **117**, 9704 (2013).

[47] W. Zhang, Z. Li, P. Lu, X. Gong, Q. Song, Q. Ji, K. Lin, J. Ma, F. He, H. Zeng, and J. Wu, Photon energy deposition in strong-field single ionization of multielectron molecules, Phys. Rev. Lett. **117**, 103002 (2016).

[48] R. Thissen, J. Oelwiche, J. M. Robbe, O. Ouflot, J. P. Flament, and J. H. D. Eland, Dissociations of the ethyne dication $C_2H_2^{2+}$, J. Chem. Phys. **99**, 6590 (1993).

[49] T. Osipov *et al.*, Fragmentation pathways for selected electronic states of the acetylene dication, J. Phys. B **41**, 091001 (2008).

[50] B. Gaire *et al.*, Photo-double-ionization of ethylene and acetylene near threshold, Phys. Rev. A **89**, 013403 (2014).

[51] R. Dörner, V. Mergel, O. Jagutzki, L. Spielberger, J. Ullrich, R. Moshammer, and H. Schmidt-Böcking, Cold target recoil ion momentum spectroscopy: A 'momentum microscope' to view atomic collision dynamics, Phys. Rep. **330**, 95 (2000).

[52] J. Ullrich, R. Moshammer, A. Dorn, R. Dörner, L. P. H. Schmidt, and H. Schmidt-Böcking, Recoil-ion and electron momentum spectroscopy: Reaction-microscopes, Rep. Prog. Phys. **66**, 1463 (2003).

[53] S. Pan, C. Hu, W. Zhang, Z. Zhang, L. Zhou, C. Lu, P. Lu, H. Ni, J. Wu, and F. He, Rabi oscillations in a stretching molecule, Light Sci. Appl. **12**, 35 (2023).

[54] K. Doblhoff-Dier, M. Kitzler, and S. Gräfe, Theoretical investigation of alignment-dependent intense-field fragmentation of acetylene, Phys. Rev. A **94**, 013405 (2016).

[55] X. Xie, K. Doblhoff-Dier, S. Roither, M. S. Schöffler, D. Kartashov, H. Xu, T. Rathje, G. G. Paulus, A. Baltuška, S. Gräfe, and M. Kitzler, Attosecond-recollision-controlled selective fragmentation of polyatomic molecules, Phys. Rev. Lett. **109**, 243001 (2012).

[56] X. Gong, Q. Song, Q. Ji, K. Lin, H. Pan, J. Ding, H. Zeng, and J. Wu, Channel-resolved above-threshold double ionization of acetylene, Phys. Rev. Lett. **114**, 163001 (2015).

[57] X. Gong, H. Li, P. Lu, Q. Song, Q. Ji, K. Lin, W. Zhang, J. Ma, H. Li, H. Zeng, and J. Wu, Ellipticity dependent symmetric break of doubly ionized acetylene in strong laser fields, J. Opt. **19**, 124008 (2017).

[58] A. S. Alnaser, X. M. Tong, T. Osipov, S. Voss, C. M. Maharjan, B. Shan, Z. Chang, and C. L. Cocke, Laser-peak-intensity calibration using recoil-ion momentum imaging, Phys. Rev. A **70**, 023413 (2004).

[59] S. Hughes, Breakdown of the area theorem: Carrier-wave Rabi flopping of femtosecond optical pulses, Phys. Rev. Lett. **81**, 3363 (1998).

[60] C. Hu, W. Li, W. Zhang, X. Gong, J. Wu, and F. He, Angle-resolved Rabi flopping in strong-field dissociation of molecules, Phys. Rev. A **103**, 043122 (2021).